Wave Height Spectrum From Sun Glint Patterns: An Inverse Problem

JOSUÉ ALVAREZ BORREGO

Departamento de Optica, División de Física Aplicada, Centro de Investigación Científica y de Educación Superior de Ensenada, Ensenada, Mexico

The problem of retrieving spatial information of sea surface heights from aerial images is considered. In this paper, some analytical and numerical results that relate the autocorrelation of the surface heights and those of the sun glint patterns are derived. Examples of these results are presented showing the nonlinear technique which can be applied to obtain the power spectrum of a real sea surface using aerial photographs. As a first step, two kinds of roughness spectra are presented: two roughness spectra which describe single-scale surfaces, and the Pierson-Moskowitz power spectrum which describe multiscale surfaces for a fully developed sea. Both simulations are presented in one dimension. However, a single-scale bidimensional surface is analyzed considering a Gaussian roughness spectrum. Wave height spectra are obtained from the surface height autocorrelation via a Fourier transform. The results of the model compared with the theory and the data are in quite good agreement. Under favorable conditions, it is possible to invert the relation numerically and estimate the wave height spectrum from the sun glint data.

1. INTRODUCTION

The west coast of the Baja California peninsula is exposed to wave motion which inflicts multiple damage. In Todos Santos Bay the waves frequently surpass the breakwater during the winter months, afflicting human settlements along the coast. The complexity of wave motion in deep waters, which can damage marine platforms and vessels, and in shallow waters, same that can afflict human settlements and recreational areas, has given origin to a long-term development in laboratory and field studies, the conclusions of which are used to design methodology and set bases to understand wave motion behavior.

To date, two types of instruments have been used for studying the sea surface: pressure sensors, which are installed below the sea surface, and buoys which are placed over the sea surface.

To measure the wave motion, the use of radar images and optical processing of aerial photographs has been used. The interest in wave data is manifold; one element is the inherent interest in the directional spectra of waves and how they influence the marine environment and the coastline. These wave data can be readily and accurately collected by aerial photographs of the wave sun glint patterns which show reflections of the Sun and sky light from the water and thus offer high-contrast wave images.

Four decades ago, *Barber* [1954] showed that the periodicity and directionality of waves can be estimated from the optical diffraction pattern of an image of the sea surface. After this pioneering work, photographic techniques have been used by several authors in their attempts to estimate various statistical parameters of sea surface heights.

In a series of articles, *Cox and Munk* [1954a, b, 1955] studied the distribution of intensity or glitter patterns in aerial photographs of the sea. One of their conclusions was that for constant and moderate wind speed, the probability density function of the slopes is approximately Gaussian.

This could be taken as an indication that in certain circumstances, the ocean surface could be modeled as a Gaussian random process. Similar observations by *Longuet-Higgins et al.* [1963] (cited by *Longuet-Higgins* [1962]) with a floating buoy, which filters out the high-frequency components, come considerably closer to the Gaussian distribution.

Other authors [*Stilwell*, 1969; *Stilwell and Pilon*, 1974] have studied the same problem considering a sea surface illuminated by continuous sky light with no azimuthal variations in sky radiance. Different models of sky light have been used emphasizing the existence of a nonlinear relationship between the slope spectrum and the corresponding wave image spectrum [*Peppers and Ostrem*, 1978; *Chapman and Irani*, 1982]. Simulated sea surfaces have been analyzed by optical systems to understand the optical technique in order to obtain a best qualitative information of the spectrum [*Alvarez Borrego*, 1987; *Alvarez Borrego and Machado*, 1985].

In fact, this problem has not been solved at all.

In this paper I derive some analytical and numerical results that relate the autocorrelation of the surface heights and those of the sun glint patterns. Examples of these results are presented showing the nonlinear technique which can be applied to obtain the power spectrum of a real sea surface using aerial photographs. As a first step, two kind of roughness spectra are presented: two roughness spectra that describe single scale surfaces, and the Pierson-Moskowitz frequency spectrum [*Pierson and Moskowitz*, 1964], which describes multiscale surfaces for a fully developed sea. For this last model the spectrum is determined completely by the wind speed. The Pierson-Moskowitz model has the advantage of simplicity yet yields surfaces that approximately model the ocean surface. Since the goal here is to test the nonlinear technique used for relating the autocorrelation of the sea surface heights and those of the sun glint patterns, the Pierson-Moskowitz model is suitable for the present study.

In this first step I consider surfaces that are rough in only one direction. Such surfaces are referred to as one-dimensional (1-D) surfaces. I assume the fluctuation of the surface height to be statistically Gaussian. This same con-
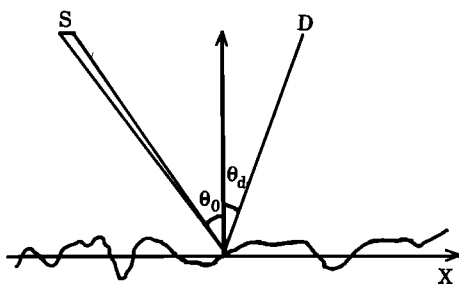
Fig. 1. Physical situation.

sideration has been made by other authors; for example, *Yang and McDaniel* [1991] and *Thorsos* [1990]. *Cox and Munk* [1956] also used the fact that the slope distribution is close to Gaussian.

I also assume that the surfaces are illuminated by a source, the Sun, of a fixed angular extent, β, and imaged through a lens that subtends a very small solid angle. With these considerations, I calculate their images, as they would be formed by a signal clipping detector. In order to do this, I define a "glitter function," which operates on the slope of the surfaces.

To test my predictions I have conducted a Monte Carlo type simulation.

Random single-scale surfaces with two different power spectra have been generated in a computer. Their "sun glint patterns" were analyzed for an incidence angle $\theta_0 = 30°$, while the detector angle θ_d was zero for the two cases.

Sun glint patterns generated by multiscale surfaces were analyzed for $\theta_0 = 20°$ and $\theta_d = 0°$, for a wind speed U of 10 m/s (19 knots). Spatial increments of 2 cm were used in the generation of the surfaces. The first two cases consisted of 16,384 points and for the last one the spatial series consisted of 131,072 points in order to see in the simulation large- and small-scale components. The apparent diameter of the Sun, β, was estimated to be 0.68°. In order to reduce statistical noise in the numerical estimation of the autocorrelation function, $C(\tau)$, of image, $L(x)$, I averaged over 400 estimated $C(\tau)$, each obtained from a different, but statistically equivalent image $L(x)$. The results are in quite good agreement with the theory and the data.

As a second step, a bidimensional surface, $Z(x, y) = (100, 100)$ matrix, was generated for its respective analysis. Spatial increments of 2 cm were used as well as 10 cm of correlation length. Considering the most simplest case, the value used for θ_0, and θ_d was zero. Nevertheless, any value can be used for both angles. In the generation of this single-scale surface, a bidimensional Gaussian roughness spectrum was used. However, for simplicity, an isotropic surface is considered. As a first approximation I describe the glitter function (which describes the sun glint patterns) as a Gaussian function which is in function of M_x and M_y (slope in x and y directions, respectively). The results presented in the x direction are in quite good agreement with the theory and the data. The same behavior was observed in the y direction.

2. DESCRIPTION AND ANALYSIS OF THE METHOD

A one-dimensional surface is illuminated by a source S of limited angular extent, and its image is formed in D (Figure 1). The incidence angle is defined as θ_0, and the apparent diameter of the source is called β. Light from the source is reflected on the surface just one time and, depending on the

slope, the light reflected will or will not be part of the image. In broad terms, the image consists of bright and dark regions that I call a "glitter pattern" and I clipped into a two-level signal. The glitter patterns obtained in the image contain spatial information of the surface.

At this point it is pertinent to note that the problem of estimated spectral information from clipped or nonlinearly detected signals has been considered by several authors in the past. In particular, we can mention the pioneering work of *Van Vleck and Middleton* [1966], and some recent applications in the context of speckle theory by *Pedersen* [1984], *Marron and Morris* [1986], and *Ohtsubo* [1985].

The situation here is somewhat different, in the sense that the clipped data depend on the geometry of the problem.

The one-dimensional surface is represented by $z = Z(x)$, assumed to be a stationary Gaussian random process with correlation $R(\tau) = \langle Z(x + \tau)Z(x)\rangle$ and variance σ_z^2. The ensemble average is represented by angle brackets. The slope is represented by $M(x)$, with correlation $Q(\tau) = \langle M(x + \tau)M(x)\rangle$ and variance σ_M^2. The relationship between $R(\tau)$ and $Q(\tau)$ is given by *Papoulis* [1981]:

$$Q(\tau) = -\frac{d^2 R(\tau)}{d\tau^2}. \tag{1}$$

From the theory of random processes, we know that with the stated assumptions, the random process $M(x)$ is Gaussian. Then the joint probability density function of slopes at two different positions x_1 and x_2 is given by

$$p(M_1, M_2) = \frac{1.0}{2\pi\sigma_M^2[1.0 - Q^2(\tau)]^{1/2}}$$

$$\cdot \exp\left[-\frac{M_1^2 + M_2^2 - 2Q(\tau)M_1 M_2}{2\sigma_M^2[1.0 - Q^2(\tau)]}\right], \tag{2}$$

where, for simplicity, I write $M(x_1)$ as M_1, and $M(x_2)$ as M_2.

The output image formed in D is a two-level random process that I denoted by $L(x)$. In general, the correlation function of this output is a function of position, but assuming that the field of view is sufficiently small that we can consider that the process is stationary over the region of interest. Then the correlation function of the process $L(x)$ can be written as $C(\tau) = \langle L(x + \tau)L(x)\rangle$, and its variance can be written as σ_L^2.

Figure 2 shows the geometry of the experiment when a one-dimensional tilted flat surface is analyzed. In this figure, α represents the angle between the x axis and the surface, θ_d
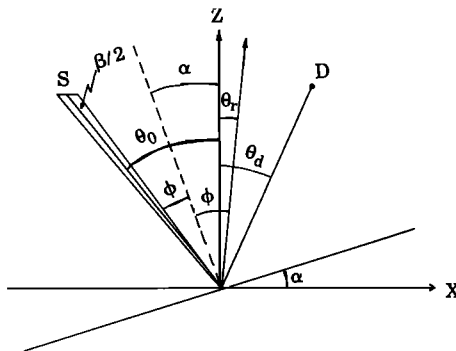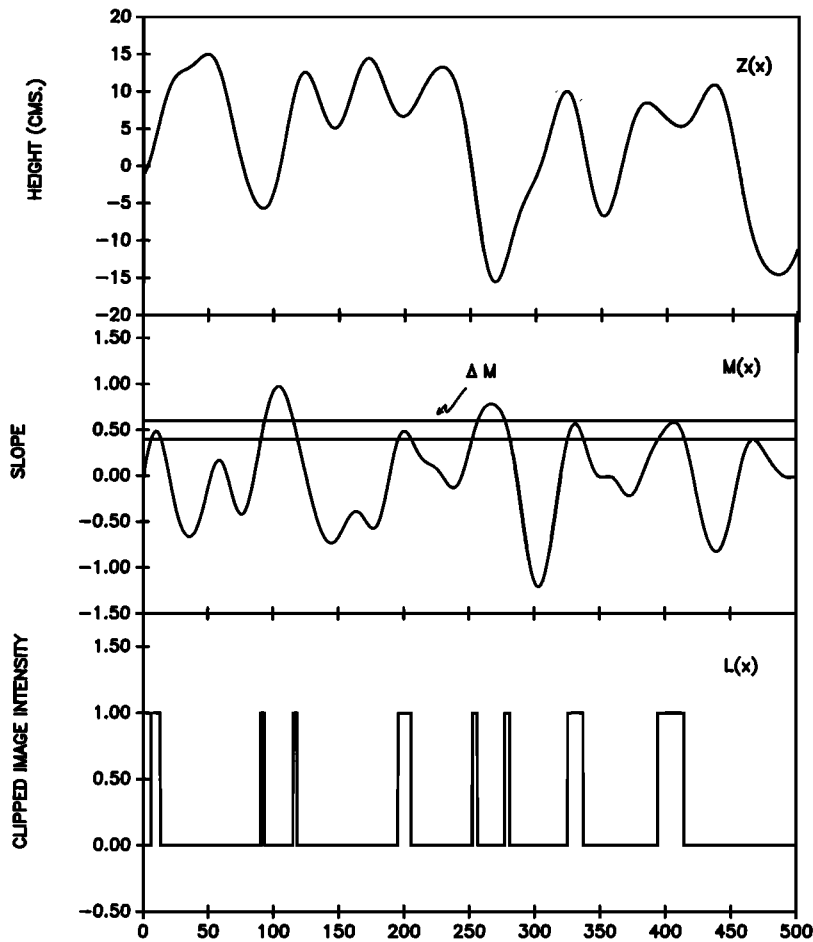

Fig. 2. Geometry of the experiment.

Fig. 3. All the processes involved showing the region selected by $B(M)$.

is the angle between the normal and the detector, and θ_0 is the angle between the normal and the source. The angular subtenses of the source and detector are represented by β and δd, respectively.

From this figure one can determine the range of angles that reflect specularly toward the detector. This is what I have called the brightness function $B(M)$ that operates on the local slope. In practical situations, δd is much smaller than β, and, taking into account the stated nonlinearity, the brightness function can be approximated by

$$B(M) = \text{rect}\left[\frac{M - M_0}{(1 + M_0^2)(\beta/2)}\right], \qquad (3)$$

where $M = \tan (\alpha)$ and $M_0 = \tan [(\theta_0 - \theta_d)/2]$. See Appendix A.

According to the glitter function $B(M)$, we can see a region selected by it in the slope data, which generate the clipped data, $L(x)$. The complete process is shown in Figure 3.

With the aforementioned considerations, the correlation of the output $L(x)$ can be written as

$$C(\tau) = \int_{-}^{+} \int_{\infty}^{\infty} \frac{B(M_1)B(M_2)}{2\pi\sigma_M^2[1.0 - Q^2(\tau)]^{1/2}}$$

$$\cdot \exp\left[-\frac{M_1^2 + M_2^2 - 2Q(\tau)M_1M_2}{2\sigma_M^2[1.0 - Q^2(\tau)]}\right] dM_1\, dM_2, \qquad (4)$$

which can be integrated numerically in order to obtain the relationship between $C(\tau)$ and $Q(\tau)$.

In essence, the technique presented here consist of first, finding a relation between σ_L^2 and σ_Z^2 and $C(\tau)$ and $R(\tau)$. Then, explore the possibilities of inverting this data. The spectrum is obtained via a Fourier transform of R. In the next section, (2) and (4) are extended to two dimensions. A relationship between the autocorrelation function of the image, $C(\xi, \eta)$, and the autocorrelation function of the surface, $R(\xi, \eta)$ is obtained.

3. RESULTS AND DISCUSSION

The $C(\tau)$-$Q(\tau)$ relation (equation 4) can be seen in Figure 4. This figure contains two plots of C versus Q for two different values of σ_M and some incidence angles.

The inversion of this relationship is possible under favorable conditions. For instance, when $\sigma_M = 0.2121$, the incidence angles from $0°$ to $10°$ are not adequate for the inversion because they give a multivalued relation. But, if I use different angle for θ_d, I can use these values. Thus depending on the incidence and the viewing angles, I obtain a good relationship for C and Q. However, when σ_M increases, the C-Q relationship changes.

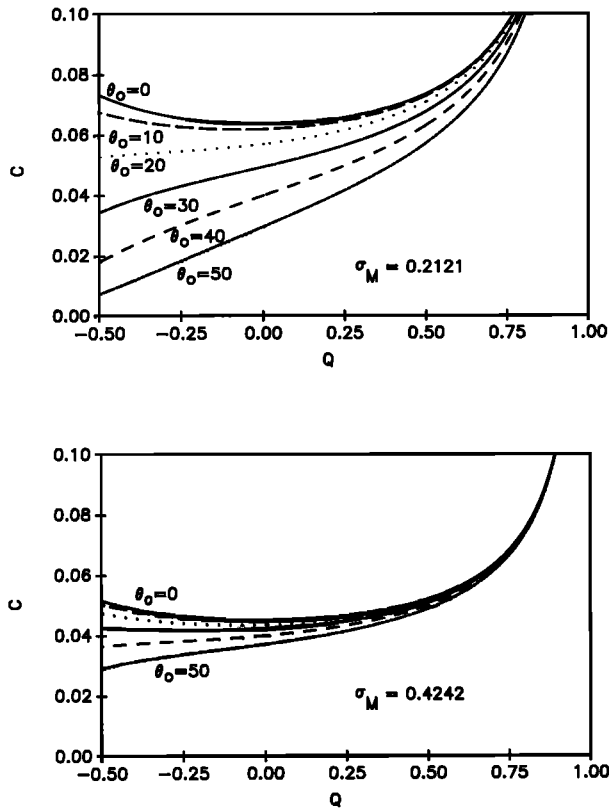The two roughness spectra which generate the single-scale one-dimensional surface, the Pierson-Moskowitz power

Fig. 4. C-Q relationship.

spectrum for a fully developed sea, and the two-dimensional surface case are described.

3.1. Single-Scale One-Dimensional Surface Generation

In order to generate surface height functions $Z(x)$ consistent with a given roughness spectrum and obeying Gaussian statistics, I used the spectral method described by *Thorsos* [1988]. For the present work, two different spectra were used, Gaussian and rectangle:

$$S_1(K_x) = l\pi^{1/2}\sigma_z^2 \exp\left[\frac{-K_x^2 l^2}{4}\right], \tag{5}$$

$$S_2(K_x) = l\sigma_z^2 \operatorname{rect}[lK_x], \tag{6}$$

where the parameter l may be identified with the correlation length, K_x is the wave number and S is the spectrum function.

I defined rect (x) as

$$\operatorname{rect}\left[\frac{x-x_0}{b}\right] = 0 \qquad \left|\frac{x-x_0}{b}\right| > \frac{1}{2},$$

$$\operatorname{rect}\left[\frac{x-x_0}{b}\right] = 1 \qquad \left|\frac{x-x_0}{b}\right| < \frac{1}{2}.$$

The corresponding correlation functions are

$$R_1(\tau) = \sigma_z^2 \exp[-\tau^2/l^2], \tag{7}$$

$$R_2(\tau) = \sigma_z^2 \operatorname{sinc}[\tau/l], \tag{8}$$

where sinc $x = \sin \pi x/\pi x$ and τ is the lag variable.

The spectra defined by (5) and (6) are used because their

autocorrelation functions are easier to obtain via a Fourier transform, and the comparison among the inversion processes, the numerical simulation, and the analytical formula can be done (Figures 5a and 6a).

From (1) I have that

$$\sigma_M = 2^{1/2}\frac{\sigma_z}{l}, \tag{9}$$

for the correlation function given by (7), but for (8) I find that

$$\sigma_M = \frac{\pi}{3^{1/2}}\frac{\sigma_z}{l}. \tag{10}$$

Now, the variance of the process $L(x)$ is given by the expression

$$\sigma_L^2 = \int_{-\infty}^{+\infty} [B(M) - \mu_L]^2 p(M) \, dM, \tag{11}$$

where μ_L, represents the mean of $L(x)$, $p(M)$ is the probability density function in one dimension, and $B(M)$ is the glitter function, which I approximate by a rect function. So I can write

$$\sigma_L^2 = \frac{1.0}{\sigma_M(2\pi)^{1/2}} \int_{-\infty}^{+\infty} \left[\operatorname{rect}\left(\frac{M-M_0}{(1+M_0^2)(\beta/2)}\right) - \mu_L\right]^2$$

$$\cdot \exp\left[-\frac{M^2}{2\sigma_M^2}\right] dM. \tag{12}$$

Defining $a = M_0 - (1 + M_0^2)(\beta/4)$ and $b = M_0 + (1 + M_0^2)(\beta/4)$, and after a suitable change of variable I find

$$\sigma_L^2 = (1 - 2\mu_L)\left[\operatorname{erf}\left(\frac{b}{\sigma_M}\right) - \operatorname{erf}\left(\frac{a}{\sigma_M}\right)\right] + \mu_L^2, \tag{13}$$
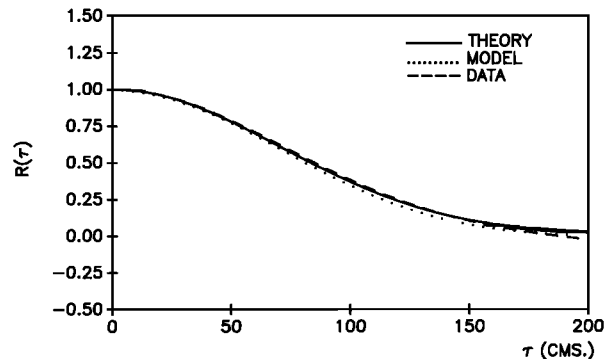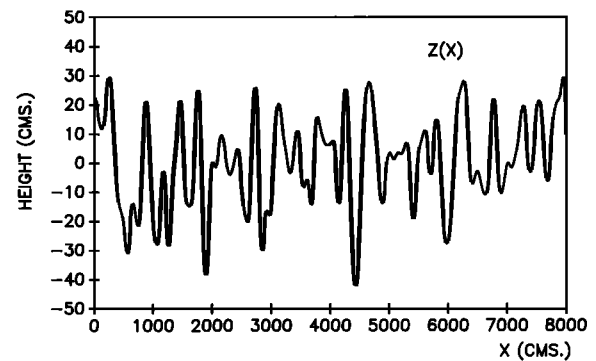
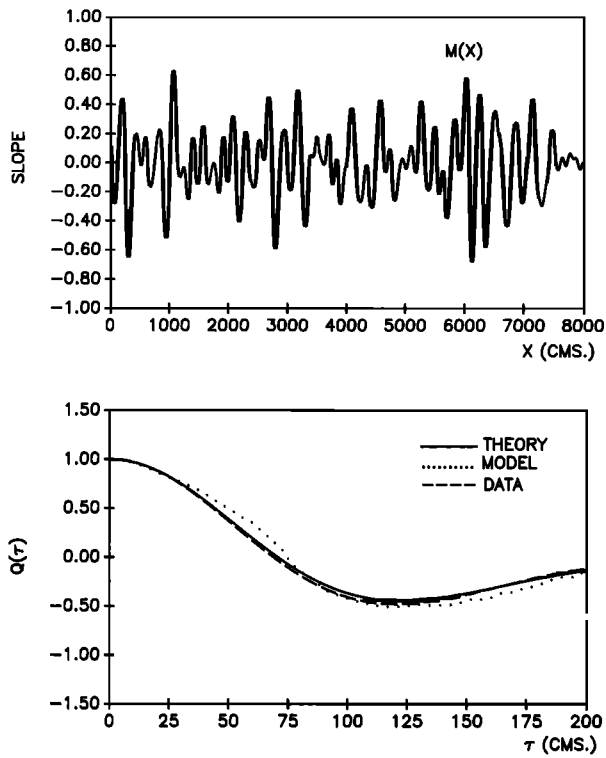Fig. 5a.   Single-scale surface $Z(x)$ and its correlation function.

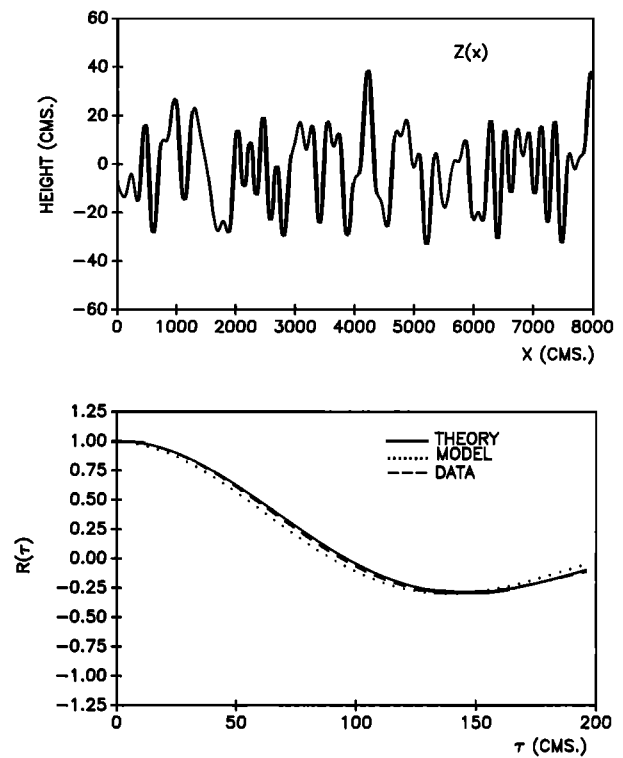Fig. 5b. Slope $M(x)$ and its correlation function.

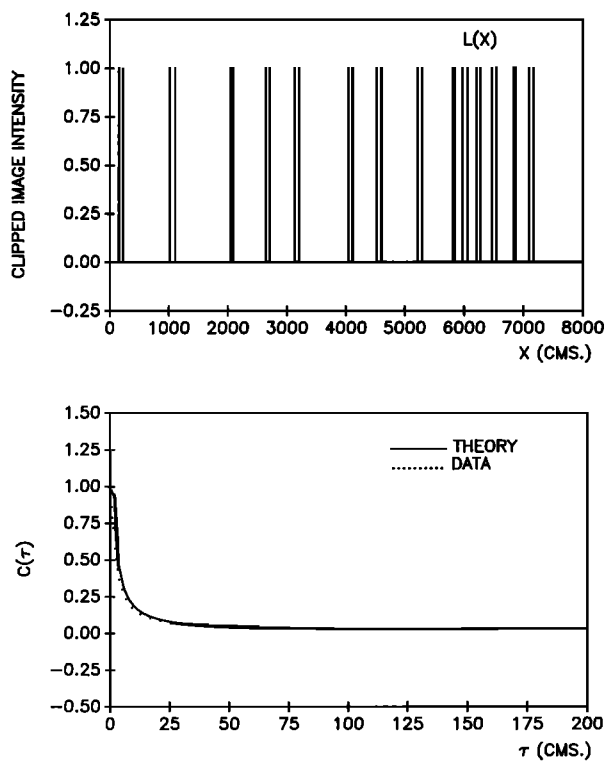Fig. 6a. Surface $Z(x)$ and its correlation function.

Fig. 5c. Image $L(x)$ and its correlation function.
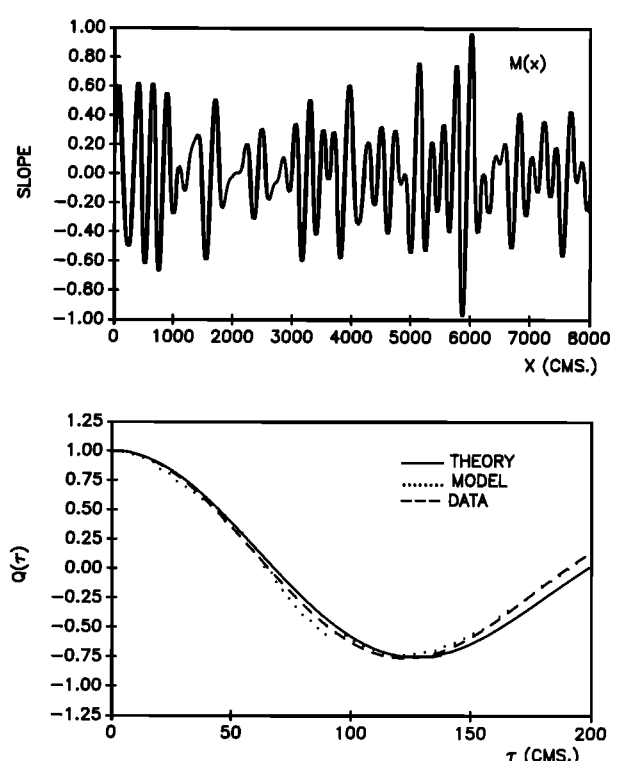

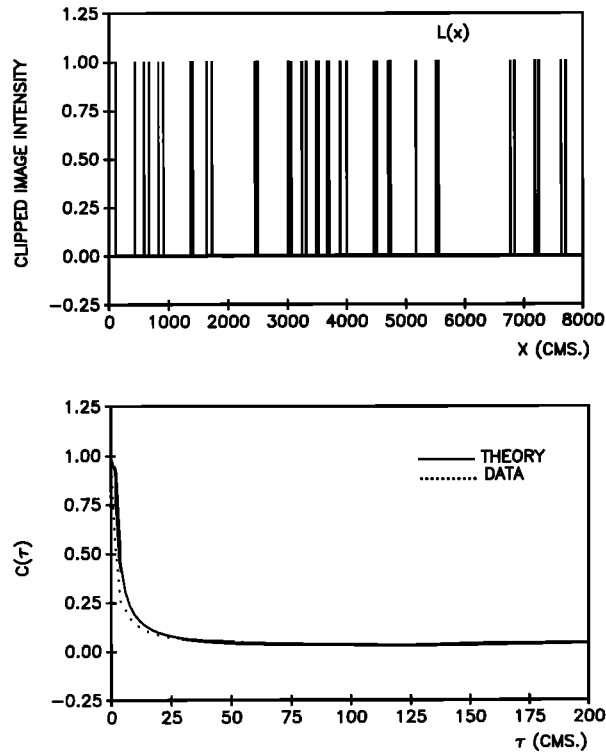Fig. 6b. Slope $M(x)$ and its correlation function.

Fig. 6c.　Image, $L(x)$ and its correlation function.

which provides the required relationship between σ_L and σ_M.

Examples of surface realizations are shown in Figures 5 and 6, corresponding to different roughness spectra given by eqs. (5) and (6), respectively. However, Figures 5 and 6 show us sample functions of $Z(x)$, $M(x)$, and $L(x)$ with their respective correlation functions, which are evaluated theoretically (solid line), from the numerically generated data (dashed line) and from the inverted data (dotted line). As can be observed, the results are in quite good agreement.

Each surface realization $Z(x)$ consisted of 16,384 points with steps of 2 cm. The parameter β, corresponding to the Sun's apparent diameter, was estimated to be $0.68°$. The angle θ_0 was considered to be $30°$, while the angle θ_d was zero for the two cases. Values of the angle α are shown in Figures 5b and 6b, represented by $M(x)$; in fact $M(x) = \tan \alpha$.

In order to reduce statistical noise in the numerical estimation of C, I averaged over 400 estimated correlation functions, each obtained from a different, but statistically equivalent $L(x)$. We can observe that the C correlations must be very well fitted, because when τ increases the relation between C and Q is very sensitive to small errors in the estimation of C.

Figure 7 shows the corresponding wave spectra obtained from the heights autocorrelation function. We can observe that for large wave numbers, the results of the inversion process (points) with the spectra obtained from the numerical simulation (dashed line) have a better agreement than with the analytical theory (solid line), because the first one was obtained from the image autocorrelation which was made considering the numerical simulation.

We can see some fluctuations in this result, as only 1024 values from the autocorrelation function were used to obtain

such spectra. So these fluctuations can be reduced in the same way that the statistical noise were reduced from the image autocorrelation.

3.2.　Multiscale One-Dimensional Surface Generation Using the Pierson-Moskowitz Model

To obtain the 1-D spectral density $S(K_x)$, I begin with the Pierson-Moskowitz frequency spectrum [Pierson and Moskowitz, 1964] given by

$$\hat{E}(w) = \frac{a_0 g^2}{w^5} \exp\left[-b_0\left(\frac{g}{wU}\right)^4\right], \qquad (14)$$

where w is the temporal frequency of the surface waves, $a_0 = 8.10 \times 10^{-3}$, $b_0 = 0.74$, $g = 9.81$ m/s^2, and U is the wind speed at a height of 19.5 m. The power spectrum (14) can be written as a function of the wave number component (K_x) for the 1-D case. The gravity wave dispersion relation

$$w^2 = g|K_x| \qquad (15)$$

is used to relate $\hat{E}(w)$ to a spatial spectral density. Using (15), I obtain

$$\hat{S}(K_x) = \hat{E}(w)J(w, K_x) = \hat{E}(gK_x)^{1/2} \frac{(g/K_x)^{1/2}}{2}, \qquad (16)$$

for $K_x > 0$ and $\hat{S}(K_x) = 0$ for $K_x < 0$, and $J(w, K_x)$ is the Jacobian given by dw/dK_x.

The simulation of the surfaces requires even spectra. For my purpose, the surface can be considered "frozen" and $S_3(K_x)$ is defined as an even function of K_x. With this consideration we can define according to Chapman [1980]
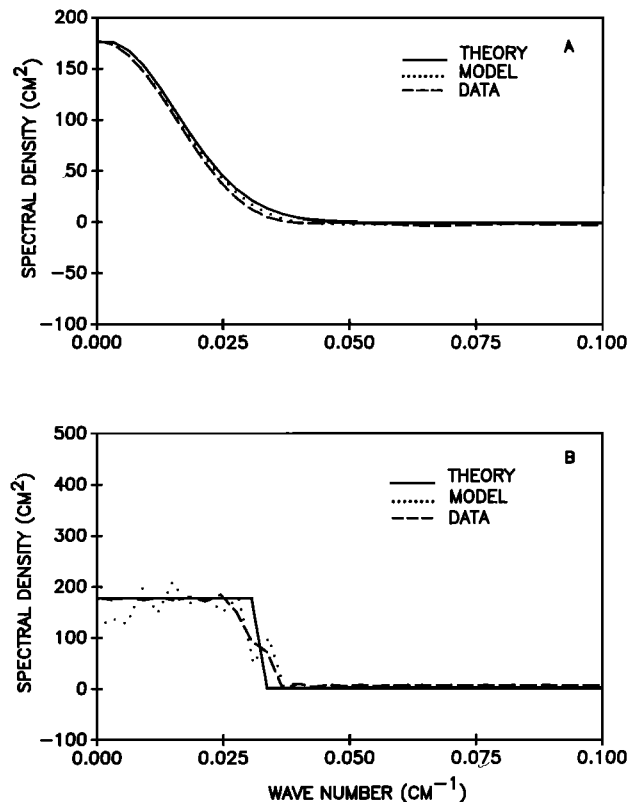

Fig. 7.　Wave height spectra for the processes of (a) Figure 5 and (b) Figure 6.

$$S_3(K_x) = \tfrac{1}{2}\, \hat{S}(K_x) \qquad K_x \geq 0,$$

$$\hspace{3cm}(17)$$

$$S_3(K_x) = \tfrac{1}{2}\, \hat{S}(-K_x) \qquad K_x < 0,$$

obtaining the spatial roughness spectrum

$$S_3(K_x) = \left[\frac{a_0}{4|K_x|^3}\right] \exp\left[-\frac{b_0 g^2}{K_x^2 U^4}\right], \qquad (18)$$

where K_x is the surface wave spatial wave number defined for positive and negative values. By converting the Pierson-Moskowitz frequency spectrum into the one-dimensional wave number spectrum given by (18), the total wave energy in the Pierson-Moskowitz wave model was applied to waves propagating along the x axis as has been done in the past [*Thorsos*, 1990; *Negrete Regagnon and Alvarez Borrego*, 1990; *Peón González and Alvarez Borrego*, 1990]. In a two-dimensional wave model, the wave energy must also be distributed in azimuth [*Thorsos*, 1990; *Negrete Regagnon and Alvarez Borrego*, 1990].

The corresponding correlation function for (18) is described by *Fortuit and De Boer* [1971] and *Peón González* [1988]. Using (13), a relationship between σ_L and σ_M can be found. However, (1) give us a relationship between σ_M and σ_Z.

Figure 8 shows examples of surface $(Z(x))$, slope $(M(x))$, and image $(L(x))$, realizations with their respective correlation functions. Spatial increments of 2 cm were used in the generation of the surface (Figure 8a). The spatial series consisted of 131,072 points in order to see in the simulation large- and small-scale components. Figure 8a shows only a short part of the series owing to space limitation. Figure 8b (slope) shows a shorter part than Figure 8a because $Z(x)$ is
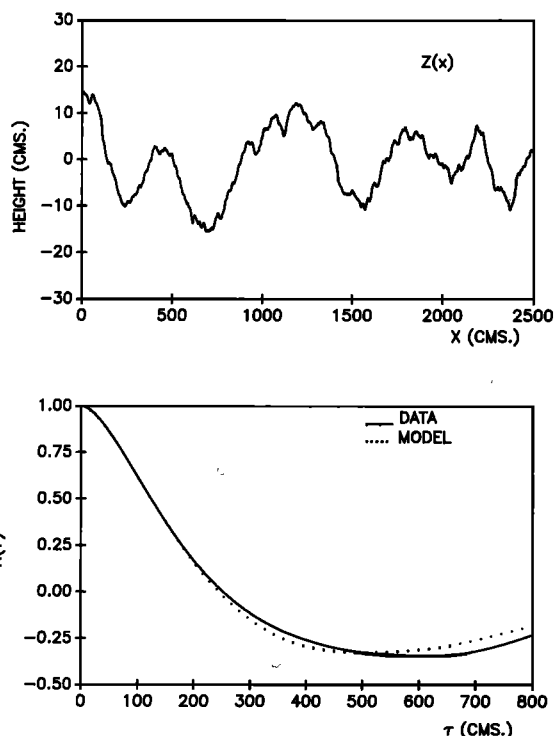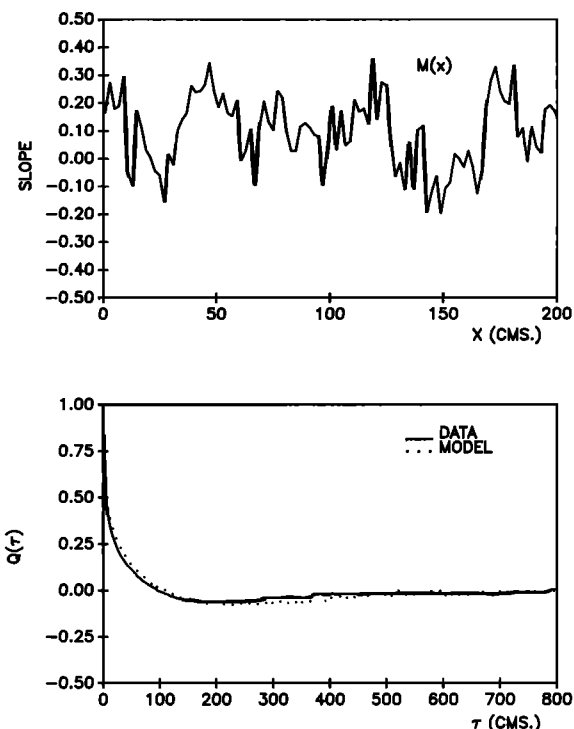
Fig. 8b. Slope $M(x)$ and its correlation function.

a multiscale surface and more fluctuations in the slope series are found. With respect to the correlations I find a quite good agreement with the data and the model. As in the 3.1 case I averaged over 400 estimated correlations functions, $C(\tau)$, in order to reduce statistical noise. The calculus computation was made on a Sun computer.

Figure 9 shows the corresponding wave spectra obtained

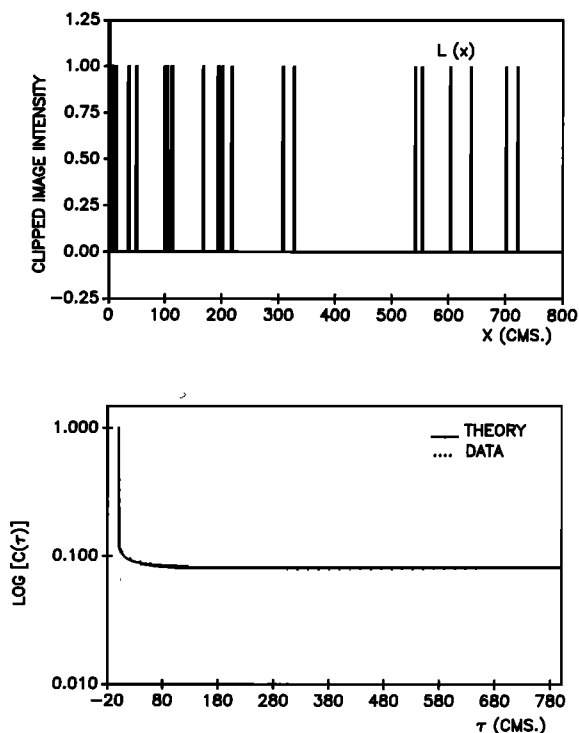Fig. 8a. Multiscale surface $Z(x)$ and its correlation function.

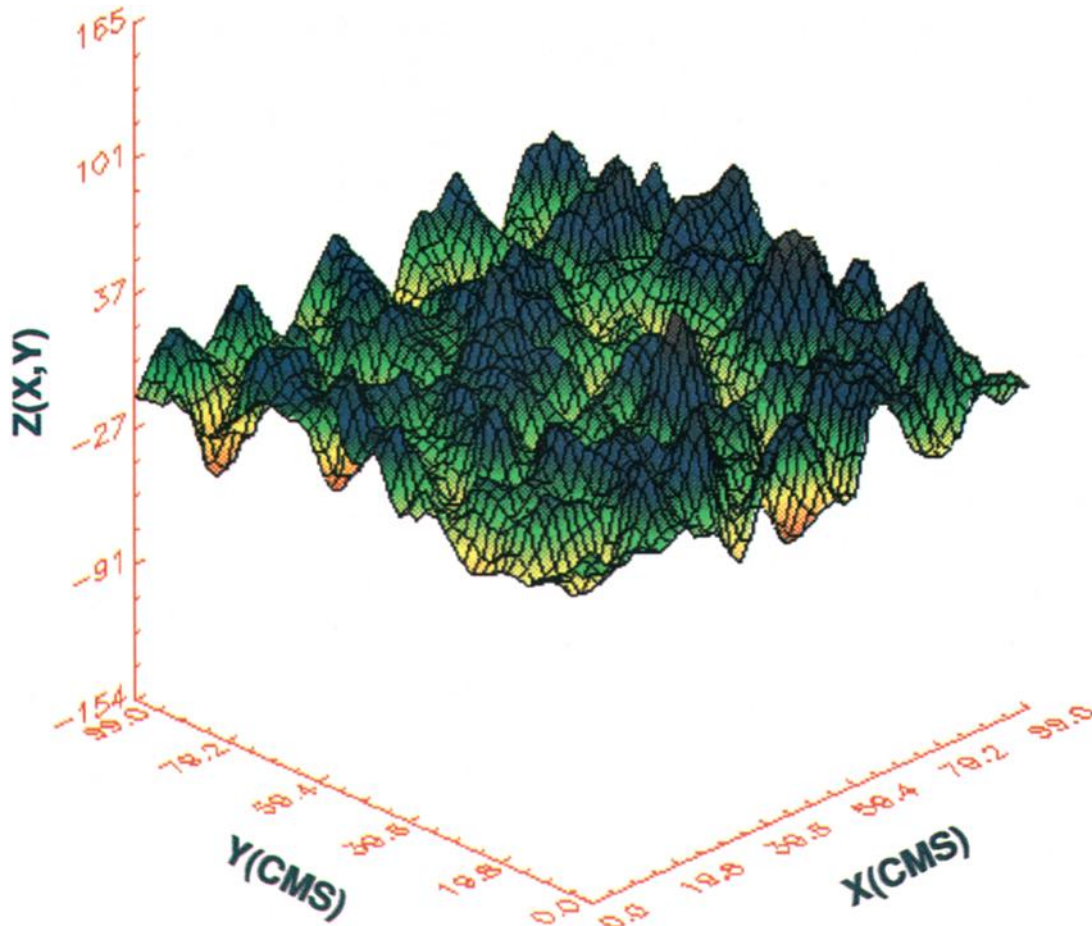Fig. 8c. Image $L(x)$ and its correlation function.

Plate 1. Single-scale bidimensional surface $Z(x, y)$.

from the height autocorrelation function. We can see a small difference only to the end of the slope of the spectra. However, the results of the model are within the 95% confidence interval of the spectra.

3.3. Single-scale Bidimensional Surface Generation

In the same way as the 1-D case, the bidimensional surface was generated using the spectral method described by *Thorsos* [1988]. A bidimensional Gaussian roughness spectrum was also used. I can write

Fig. 9. Wave height spectrum for the process of Figure 8 with 95% confidence interval.

$$S_4(K_x, K_y) = \sigma_Z^2 (\pi l_x l_y)^{1/2} \exp\left[-\frac{\pi^2(K_x^2 l_x^2 + K_y^2 l_y^2)}{2}\right],$$
(19)

where K is the bidimensional wave number defined as $K^2 = K_x^2 + K_y^2$, l_x and l_y are the correlation length in the x and y directions respectively, and S_4 is the bidimensional spectral density function.

The corresponding correlation function of the surface is given by

$$R_4(\xi, \eta) = \sigma_Z^2 \exp\left[-\left(\frac{\xi^2}{l_x^2} + \frac{\eta^2}{l_y^2}\right)\right],$$
(20)

where ξ and η are the lag variable in the x and y direction, respectively. However, for an isotropic surface $l_x = l_y = l$, so we can write (20) as

$$R_4(\xi, \eta) = \sigma_Z^2 \exp\left[-\frac{(\xi^2 + \eta^2)}{l^2}\right].$$
(21)

Appendix B shows the relationships between $R_4(\xi, \eta)$ and $Q^x(\xi, \eta)$ (autocorrelation function of the slope in x direction), $Q^y(\xi, \eta)$ (autocorrelation function of the slope in y direction) and $Q^{xy}(\xi, \eta)$ (cross-correlation function between the x and y slopes), respectively. These relationships can be written as
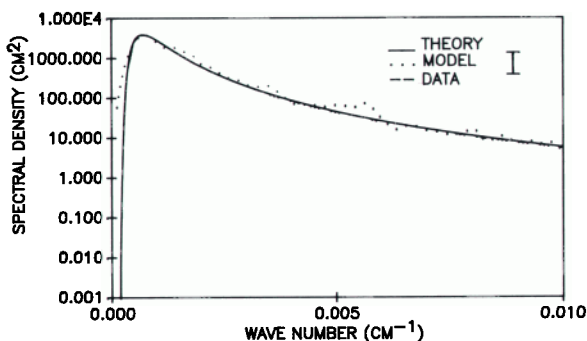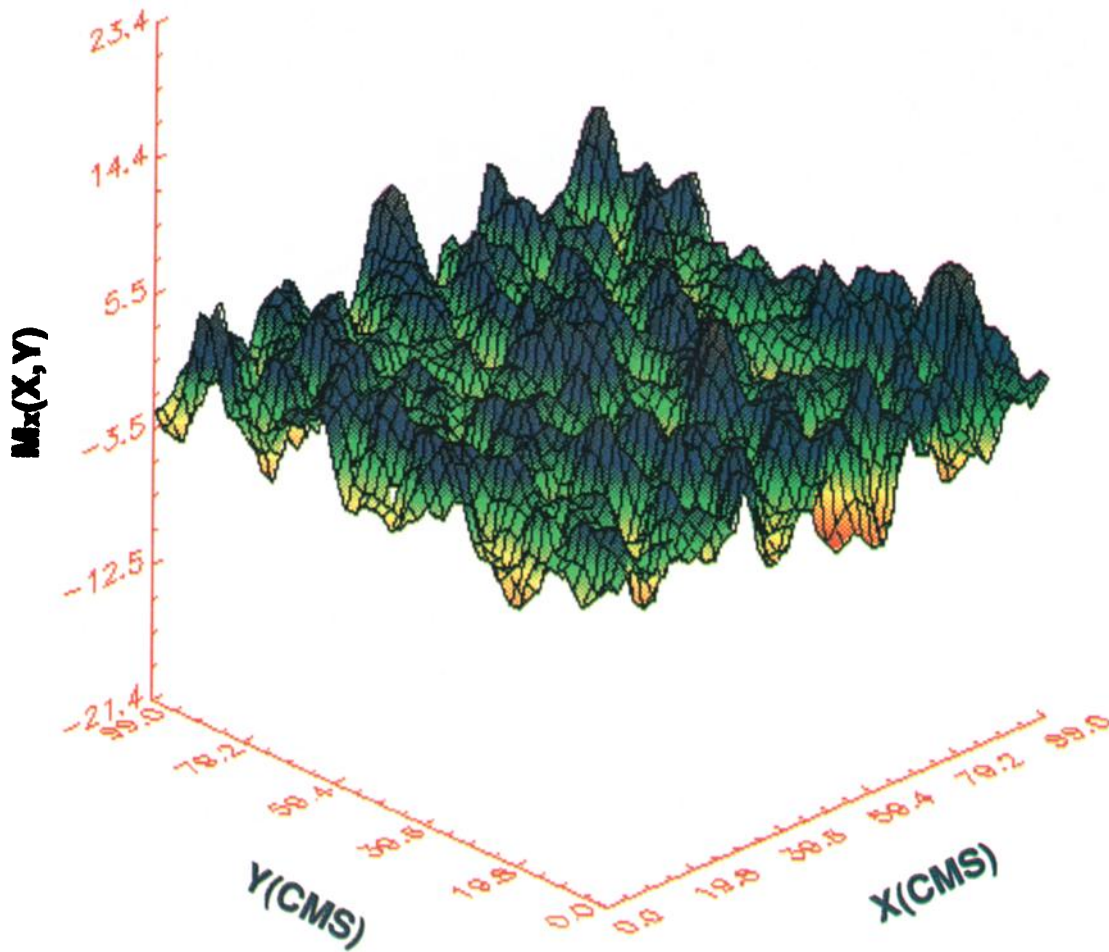
Plate 2. Slope $M_x(x, y)$.

$$\langle M_x(x + \xi, y + \eta)M_x(x, y)\rangle = Q^x(\xi, \eta)$$

$$= -\left(\frac{4\xi^2}{l^4} - \frac{2}{l^2}\right)R_4(\xi, \eta), \qquad (22)$$

$$\langle M_y(x + \xi, y + \eta)M_y(x, y)\rangle = Q^y(\xi, \eta)$$

$$= -\left(\frac{4\eta^2}{l^4} - \frac{2}{l^2}\right)R_4(\xi, \eta), \qquad (23)$$

$$\langle M_x(x + \xi, y + \eta)M_y(x, y)\rangle = Q^{xy}(\xi, \eta)$$

$$= -\frac{4\xi\eta}{l^4} R_4(\xi, \eta). \qquad (24)$$

As we can see in the (22) and (23), the relationship between σ_M and σ_Z when we have an isotropic surface is the same as (9).

Considering Gaussian statistics as in one dimensional case we have that the probability density function of slopes at two different positions x_1, x_2, and y_1, y_2, is given by [*Davenport and Root*, 1958]

$$p(M_x, M_y, M_{x'}, M_{y'}) = \frac{1}{4\pi^2|\Lambda|^{1/2}}$$

$$\cdot \exp\left[-\frac{1}{2|\Lambda|} \sum_{n=1}^{4} \sum_{m=1}^{4} |\Lambda|_{nm}(M_n - \mu_n)(M_m - \mu_m)\right], \qquad (25)$$

where, for simplicity, I write $M(x_1)$ as M_x, $M(x_2)$ as $M_{x'}$, $M(y_1)$ as M_y and $M(y_2)$ as $M_{y'}$; μ_n or μ_m represents the mean of $M(x, y)$; and $|\Lambda|_{nm}$ is the cofactor of the element λ_{nm} in the determinant $|\Lambda|$ of the covariance matrix

$$\Lambda = \begin{bmatrix} \lambda_{11} & \lambda_{12} & \cdots & \lambda_{1N} \\ \lambda_{21} & \lambda_{22} & \cdots & \lambda_{2N} \\ \vdots & \vdots & \vdots & \vdots \\ \lambda_{N1} & \lambda_{N2} & \cdots & \lambda_{NN} \end{bmatrix} = \begin{bmatrix} \sigma_M^2 & 0 & Q^x & Q^{xy} \\ 0 & \sigma_M^2 & Q^{xy} & Q^y \\ Q^x & Q^{xy} & \sigma_M^2 & Q^{xy} \\ Q^{xy} & Q^y & Q^{xy} & \sigma_M^2 \end{bmatrix}. \qquad (26)$$

The determinant is given as

$$|\Lambda| = \sigma_M^8 - \sigma_M^4(Q^{x^2} + Q^{y^2}) - 3\sigma_M^4 Q^{xy^2} + 2\sigma_M^2 Q^{xy^2} Q^y$$

$$+ \sigma_M^2 Q^{xy^2}(1 + Q^x) + (Q^x Q^y - Q^{xy^2})^2. \qquad (27)$$

The cofactors are defined as
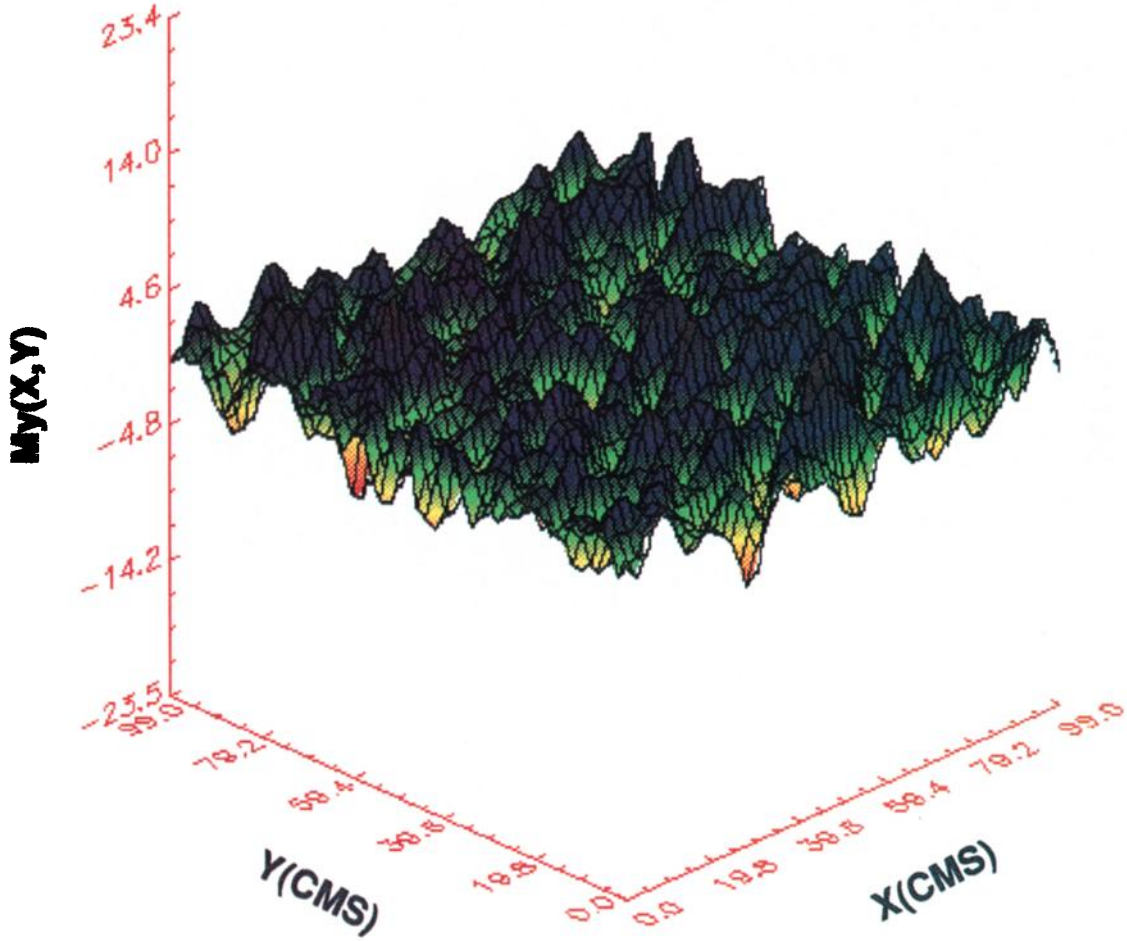
Plate 3. Slope $M_y(x, y)$.

$$|\Lambda|_{11} = \sigma_M^6 - \sigma_M^2 Q^{y^2} + 2Q^{xy^2}(Q^y - \sigma_M^2),$$

$$|\Lambda|_{22} = \sigma_M^6 - \sigma_m^2 Q^{x^2} + 2Q^{xy^2}(Q^x - \sigma_M^2),$$

$$|\Lambda|_{33} = \sigma_M^6 - \sigma_M^2 Q^{y^2} - \sigma_M^2 Q^{xy^2},$$

$$|\Lambda|_{44} = \sigma_M^6 - \sigma_m^2 Q^{x^2} - \sigma_M^2 Q^{xy^2},$$

$$|\Lambda|_{12} = |\Lambda|_{21} = Q^{xy}(Q^{xy^2} - \sigma_M^2 Q^x + Q^x Q^y - \sigma_M^2 Q^y),$$

$$|\Lambda|_{13} = |\Lambda|_{31} = Q^{xy^2}(\sigma_M^2 - Q^y) - Q^x(\sigma_M^4 - Q^{y^2}),$$

$$|\Lambda|_{14} = |\Lambda|_{41} = Q^{xy}(\sigma_M^4 - \sigma_M^2 Q^x + Q^x Q^y - Q^{xy^2}),$$

$$|\Lambda|_{23} = |\Lambda|_{32} = Q^{xy}(\sigma_M^4 - \sigma_M^2 Q^y + Q^x Q^y - Q^{xy^2}),$$

$$|\Lambda|_{24} = |\Lambda|_{42} = Q^{xy^2}(\sigma_M^2 - Q^x) - Q^y(\sigma_M^4 - Q^{x^2}),$$

$$|\Lambda|_{43} = |\Lambda|_{34} = \sigma_M^2 Q^{xy}(\sigma_M^2 - Q^y - Q^x).$$

The bidimensional glitter function is defined as

$$B(M_x, M_y) = \exp\left[-\frac{(M_x - \theta_0)^2 + (M_y - \theta_0)^2}{a^2}\right], \quad (28)$$

where θ_0, for this case, was considered to be zero, and a^2 gives us the width of the Gaussian function. The value a^2 gives us a physical situation similar to β.

With the considerations given above, the correlation of the output $L(x, y)$ can be written as

$$C(\xi, \eta) = \int\int\int\int_{-\infty}^{+\infty} B(M_x, M_y)B(M_{x'}, M_{y'})$$

$$\cdot p(M_x, M_y, M_{x'}, M_{y'}) \, dM_x \, dM_y \, dM_{x'} \, dM_{y'}, \quad (29)$$

which can be integrated analytically in order to obtain the relationship between $C(\xi, \eta)$ and $R(\xi, \eta)$. See Appendix C.

Plates 1–4 show the bidimensional surface $Z(x, y)$; the slope in the x direction, $M_x(x, y)$; the slope in the y direction, $M_y(x, y)$; and the image $L(x, y)$ obtained with the glitter function (equation (28)) when $\theta_0 = \theta_d = 0$, respectively. Figure 10b shows us the comparison of the theory with the data of the autocorrelation function of the image, $C(\xi, \eta)$, in ξ (x direction), for one realization only. Figure 10a shows us the comparison of the theory, data and model of the autocorrelation function of the surface, $R(\xi, \eta)$, in the ξ direction, for 400 ensemble average realizations. Figure 11
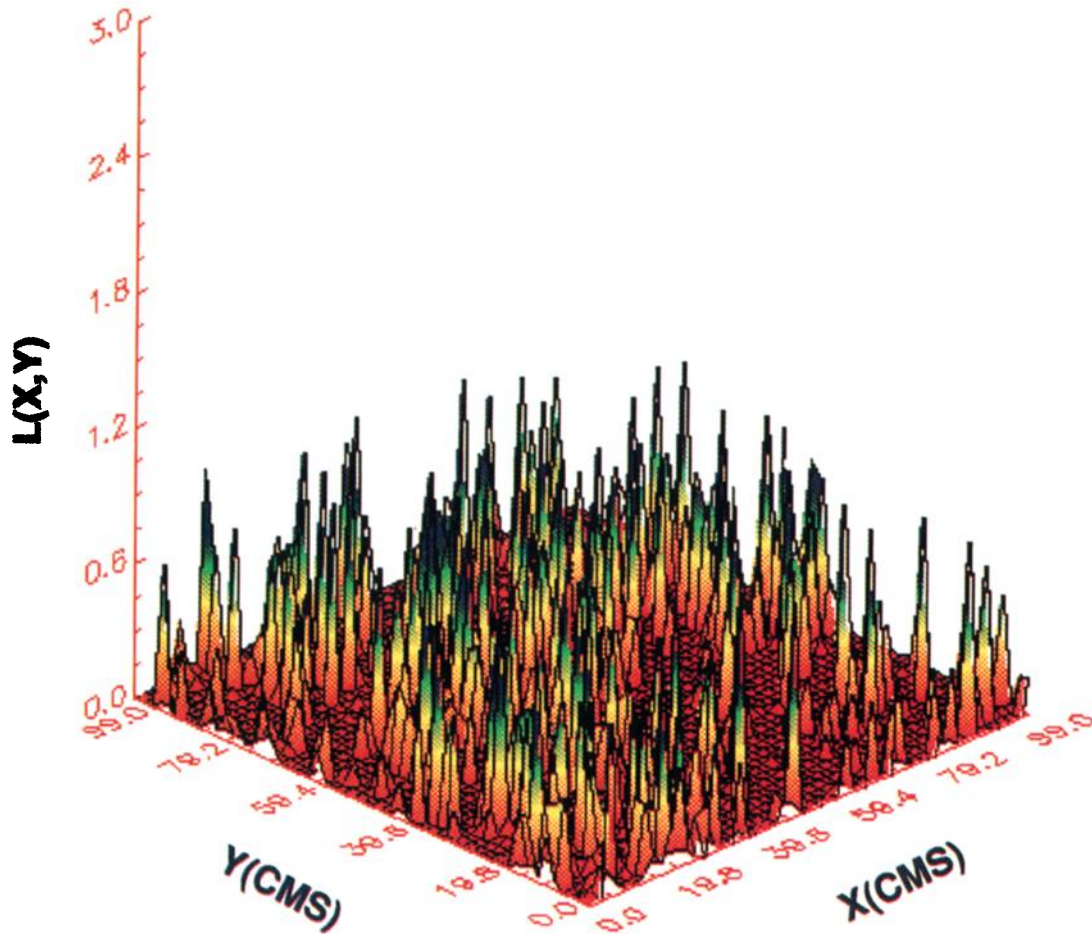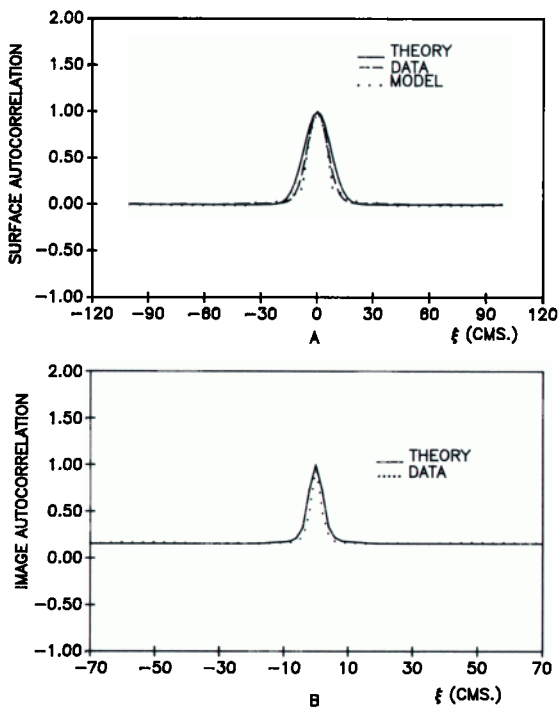
Plate 4. Image $L(x, y)$.

Fig. 10. (*a*) Autocorrelation function of the surface $R(\xi, \eta)$ in ξ direction. (*b*) Autocorrelation function of the image $C(\xi, \eta)$ in ξ direction.

gives us a graphic representation of the analytical relationship of the image autocorrelation $C(\xi, \eta)$ with the surface autocorrelation $R(\xi, \eta)$ (equation (29)). The results in η (y direction) are not shown because as it is an isotropic surface, the results obtained had the same behavior as those for the ξ direction.

4. CONCLUSION

Wave height spectra from sun glint patterns were found. This was possible via a Fourier transform of the surface height autocorrelation.
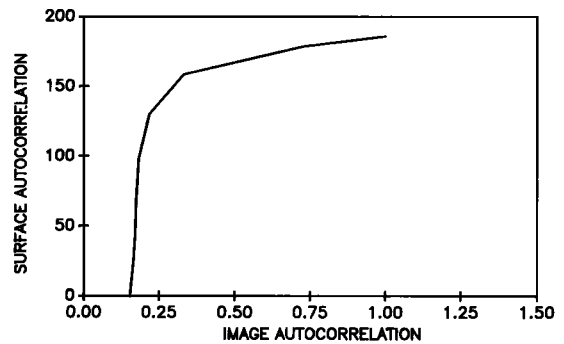

Fig. 11. $C(\xi, \eta)$-$R(\xi, \eta)$ relationship.

To obtain this result, a numerical relation between the surface height autocorrelation and the autocorrelation of the intensity variations in the photographic image was found.

APPENDIX A

Consider Figure 2, where α represents the angle between the x axis and the surface, and ϕ represents the angle between the normal to the plane and the source (S). The incidence angle is given by $\phi = \theta_0 - \alpha$, and the specular angle is given by $\phi = \theta_r + \alpha$. From this two equations we can write

$$\theta_r = \theta_0 - 2\alpha.$$

The angular dimension, θ_s, of the Sun is

$$\theta_0 - \frac{\beta}{2} \le \theta_s \le \theta_0 + \frac{\beta}{2},$$

where β is defined as in the text.

With this range, I can write the unidimensional source as

$$\text{rect}\left[\frac{\theta_s - \theta_0}{\beta}\right].$$

So, the projection of this source on the detector, after reflection, is given by

$$\theta_0 - \frac{\beta}{2} - 2\alpha \le \theta_s - 2\alpha \le \theta_0 + \frac{\beta}{2} - 2\alpha,$$

$$\theta_r - \frac{\beta}{2} \le \theta \le \theta_r + \frac{\beta}{2},$$

where $\theta = \theta_s - 2\alpha$.

The reflection will arrive to the detector (D) when

$$\theta_r - \frac{\beta}{2} \le \theta_d \le \theta_r + \frac{\beta}{2},$$

$$\frac{\theta_0 - \theta_d}{2} - \frac{\beta}{4} \le \alpha \le \frac{\theta_0 - \theta_d}{2} + \frac{\beta}{4}.$$

Because I am interested in the slopes of the surface, I can write

$$\tan\left[\frac{\theta_0 - \theta_d}{2} - \frac{\beta}{4}\right] \le \tan \alpha \le \tan\left[\frac{\theta_0 - \theta_d}{2} + \frac{\beta}{4}\right],$$

and if $\gamma = (\theta_0 - \theta_d)/2$, I can say that

$$\tan\left(\gamma - \frac{\beta}{4}\right) \approx \tan \gamma - (1 + \tan^2 \gamma)\frac{\beta}{4},$$

$$\tan\left(\gamma + \frac{\beta}{4}\right) \approx \tan \gamma + (1 + \tan^2 \gamma)\frac{\beta}{4}.$$

However, if $M = \tan \alpha$ and $M_0 = \tan \gamma$, then

$$M_0 - (1 + M_0^2)\frac{\beta}{4} \le M \le M_0 + (1 + M_0^2)\frac{\beta}{4}.$$

The last expression gives us the "glitter function" in one dimension,

$$\text{rect}\left[\frac{M - M_0}{(1 + M_0^2)(\beta/2)}\right].$$

APPENDIX B

The relationship between $R_4(\xi, \eta)$ and $Q^x(\xi, \eta)$ can be written as follows:

$$\langle M_x(x + \xi, y + \eta)M_x(x, y)\rangle$$

$$= \left\langle\left\{\frac{Z(x + \xi + \Delta x, y + \eta) - Z(x + \xi, y + \eta)}{\Delta x}\right\}\right.$$

$$\left.\cdot\left\{\frac{Z(x + \Delta x, y) - Z(x, y)}{\Delta x}\right\}\right\rangle,$$

$$= \left\{\frac{1}{(\Delta x)^2}\{\langle Z(x + \xi + \Delta x, y + \eta)Z(x + \Delta x, y)\rangle\right.$$

$$- \langle Z(x + \xi + \Delta x, y + \eta)Z(x, y)\rangle - \langle Z(x + \xi, y$$

$$+ \eta)Z(x + \Delta x, y)\rangle + \langle Z(x + \xi, y + \eta)Z(x, y)\rangle\}\},$$

$$= \frac{1}{(\Delta x)^2}\{R(\xi, \eta) - R(\xi + \Delta x, \eta)$$

$$- R(\xi - \Delta x, \eta) + R(\xi, \eta)\}.$$

Using a Taylor series for $R(\xi + \Delta x, \eta)$ and $R(\xi - \Delta x, \eta)$, we have

$$R(\xi + \Delta x, \eta) = R(\xi, \eta)$$

$$+ \Delta x \frac{\partial R(\xi, \eta)}{\partial \xi} + \frac{(\Delta x)^2}{2}\frac{\partial^2 R(\xi, \eta)}{\partial \xi^2} + \cdots,$$

$$R(\xi - \Delta x, \eta) = R(\xi, \eta)$$

$$- \Delta x \frac{\partial R(\xi, \eta)}{\partial \xi} + \frac{(\Delta x)^2}{2}\frac{\partial^2 R(\xi, \eta)}{\partial \xi^2} - \cdots,$$

and making the substitution, the result will be $-\partial^2 R(\xi, \eta)/\partial \xi^2$. Therefore

$$Q^x(\xi, \eta) = \langle M_x(x + \xi, y + \eta)M_x(x, y)\rangle = -\frac{\partial^2 R(\xi, \eta)}{\partial \xi^2}.$$

The same demonstration applies for $\langle M_y(x + \xi, y + \eta)M_y(x, y)\rangle$.

For the third relationship, we can write

$$\langle M_x(x + \xi, y + \eta)M_y(x, y)\rangle$$

$$= \left\langle\left[\frac{Z(x + \xi + \Delta x, y + \eta) - Z(x + \xi, y + \eta)}{\Delta x}\right]\right.$$

$$\left.\cdot\left[\frac{Z(x, y + \Delta y) - Z(x, y)}{\Delta y}\right]\right\rangle,$$

$$= \frac{1}{\Delta x \Delta y}\{\langle Z(x + \xi + \Delta x, y + \eta)Z(x, y + \Delta y)\rangle$$

$$- \langle Z(x + \xi + \Delta x, y + \eta)Z(x, y)\rangle$$

$$- \langle Z(x + \xi, y + \eta)Z(x, y + \Delta y)\rangle$$

$$+ \langle Z(x + \xi, y + \eta)Z(x, y)\rangle\},$$

$$= \frac{1}{\Delta x \Delta y} [R(\xi + \Delta x, \eta - \Delta y) - R(\xi + \Delta x, \eta)$$

$$- R(\xi, \eta - \Delta y) + R(\xi, \eta)],$$

$$= \frac{1}{\Delta x} \left[\frac{R(\xi + \Delta x, \eta - \Delta y) - R(\xi + \Delta x, \eta)}{\Delta y} \right.$$

$$\left. + \frac{R(\xi, \eta) - R(\xi, \eta - \Delta y)}{\Delta y} \right],$$

$$= \frac{1}{\Delta x} \left[- \frac{R(\xi + \Delta x, \eta) - R(\xi + \Delta x, \eta - \Delta y)}{\Delta y} \right.$$

$$\left. + \frac{R(\xi, \eta) - R(\xi, \eta - \Delta y)}{\Delta y} \right],$$

$$= \frac{1}{\Delta x} \left[- \frac{\partial R(\xi + \Delta x, \eta)}{\partial \eta} + \frac{\partial R(\xi, \eta)}{\partial \eta} \right],$$

$$= - \left[\frac{\partial R(\xi + \Delta x, \eta)}{\partial \eta} - \frac{\partial R(\xi, \eta)}{\partial \eta} \right] \Big/ \Delta x$$

$$= - \frac{\partial^2 R(\xi, \eta)}{\partial \xi \partial \eta}.$$

$$\therefore Q^{xy}(\xi, \eta) = \langle M_x(x + \xi, y + \eta)M_y(x, y)\rangle$$

$$= - \frac{\partial^2 R(\xi, \eta)}{\partial \xi \partial \eta}.$$

APPENDIX C

In this appendix I obtain the analytical results of equation (29). I used the formula

$$\int_{-\infty}^{+\infty} \exp [-(ax^2 + bx + c)] \, dx = \left(\frac{\pi}{a}\right)^{1/2} \exp \left[\frac{b^2 - 4ac}{4a}\right].$$

So the integral

$$C(\xi, \eta) = \iiiint\limits_{-\infty}^{+\infty} B(M_x, M_y)B(M_{x'}, M_{y'})$$

$$\cdot p(M_x, M_y, M_{x'}, M_{y'}) \, dM_x \, dM_y \, dM_{x'} \, dM_{y'}$$

has the result

$$C(\xi, \eta) = \frac{\chi_0}{4|\Lambda|^{1/2}} \left[\frac{[\chi_2 - \chi_3^2][\chi_4 - \chi_5^2]}{4\chi_1} \right.$$

$$\left. - \frac{\chi_0[\chi_6\chi_7 - \chi_8\chi_5]^2}{\chi_6} \right]^{-1/2},$$

where

$$\chi_0 = 4\left(\frac{1}{a^2} + \frac{|\Lambda|_{11}}{2|\Lambda|}\right),$$

$$\chi_1 = \chi_0\left[\chi_0\left(\frac{1}{a^2} + \frac{|\Lambda|_{22}}{2|\Lambda|}\right) - \left(\frac{|\Lambda|_{12}}{|\Lambda|}\right)^2\right],$$

$$\chi_2 = 4\chi_1\left[\chi_0\left(\frac{1}{a^2} + \frac{|\Lambda|_{33}}{2|\Lambda|}\right) - \left(\frac{|\Lambda|_{13}}{|\Lambda|}\right)^2\right],$$

$$\chi_3 = \left[\chi_0 \frac{|\Lambda|_{23}}{|\Lambda|} - \frac{|\Lambda|_{12}|\Lambda|_{13}}{|\Lambda|^2}\right],$$

$$\chi_4 = 4\chi_1\left[\chi_0\left(\frac{1}{a^2} + \frac{|\Lambda|_{44}}{2|\Lambda|}\right) - \left(\frac{|\Lambda|_{14}}{|\Lambda|}\right)^2\right],$$

$$\chi_5 = \left[\chi_0 \frac{|\Lambda|_{24}}{|\Lambda|} - 2 \frac{|\Lambda|_{12}|\Lambda|_{14}}{|\Lambda|^2}\right],$$

$$\chi_6 = \left[\chi_0\left(\frac{1}{a^2} + \frac{|\Lambda|_{22}}{2|\Lambda|}\right) - \left(\frac{|\Lambda|_{12}}{|\Lambda|}\right)^2\right],$$

$$\chi_7 = \chi_0 \frac{|\Lambda|_{34}}{|\Lambda|} - 2 \frac{|\Lambda|_{13}|\Lambda|_{14}}{|\Lambda|^2},$$

$$\chi_8 = \left[\frac{\chi_0}{2} \frac{|\Lambda|_{23}}{|\Lambda|} - \frac{|\Lambda|_{12}|\Lambda|_{13}}{|\Lambda|^2}\right],$$

and the cofactors are as defined in the text.

REFERENCES

Alvarez Borrego, J., Optical analysis of two simulated images of the sea surface, *Proc. SPIE Int. Soc. Opt. Eng.*, *804*, 192–200, 1987.

Alvarez Borrego, J., and M. A. Machado, Optical analysis of a simulated image of the sea surface, *Appl. Opt.*, *24*, 1064–1072, 1985.

Barber, N. F., Finding the direction of travel of sea waves, *Nature*, *174*, 1048–1050, 1954.

Chapman, D. M. F., The directional nature of attenuation of sound due to scattering at a rough ocean surface, *J. Acoust. Soc. Am.*, *68*, 1475–1481, 1980.

Chapman, R., and G. B. Irani, Errors in estimating slope spectra from wave images, Preprint, Appl. Phys. Lab., Johns Hopkins Univ., Laurel, Md., 1982.

Cox, C., and W. Munk, Measurement of the roughness of the sea surface from photographs of the Sun's glitter, *J. Opt. Soc. Am.*, *44*, 838–850, 1954a.

Cox, C., and W. Munk, Statistics of the sea surface derived from sun glitter, *J. Mar. Res.*, *13*, 198–227, 1954b.

Cox, C., and W. Munk, Some problems in optical oceanography, *J. Mar. Res.*, *14*, 381–396, 1955.

Cox, C., and W. Munk, Slopes of the sea surface deduced from photography of Sun glitter, *Bull. Scripps Inst. Oceanogr.*, *6*(5), 397–487, 1956.

Davenport, W. B., Jr., and W. L. Root, *An Introduction to the Theory of Random Signals and Noise*, McGraw-Hill, New York, 1958.

Fortuit, L., and J. G. De Boer, Spatial and temporal correlation of the sea surface, *J. Acoust. Soc. Am.*, *49*, 1677–1679, 1971.

Longuet-Higgins, M. S., The statistical geometry of random surfaces, *Hydrodyn. Instab. Proc. Symp. Applied Math.*, *13th, 1960*, 105–143, 1962.

Longuet-Higgins, M. S., D. E. Cartwright, and N. D. Smith, Observations of the directional spectrum of sea waves—Using the motions of a floating buoy, in *Ocean Wave Spectra*, pp. 111–136, Prentice-Hall, Englewood Cliffs, N. J., 1963.

Marron, J., and G. M. Morris, Correlation measurements using clipped laser speckle, *Appl. Opt.*, *25*, 789, 1986.

Negrete Regagnon, P., and J. Alvarez Borrego, Optical and digital image processing of a simulated sea surface, *Opt. Pura Apl.*, *23*, 7–29, 1990.

Ohtsubo, J., Intensity clipping correlation of speckle patterns, *Appl. Opt.*, *24*, 746, 1985.

Papoulis, A., *Probability, Random Variables, and Stochastic Processes*, chap. 9, McGraw-Hill, New York, 1981.

Pedersen, H., Theory of speckle-correlation measurements using nonlinear detectors, *J. Opt. Soc. Am.*, *1*, 850, 1984.

Peón González, R., Correlación optica y digital de superficies marinas simuladas que contienen el espectro teórico de Pierson-Neumann y Pierson-Moskowitz, Bachelor thesis, Fac. de Cienc. Mar., Univ. Auton. de Baja Calif., Ensenada, Mexico, 1988.

Peón González, R., and J. Alvarez Borrego, Optical and digital correlation of simulated sea surfaces, *Opt. Pura Apl.*, *23*, 31–54, 1990.

Peppers, N., and J. S. Ostrem, Determination of wave slopes from photographs of the ocean surface: A new approach, *Appl. Opt.*, *17*, 3450–3458, 1978.

Pierson, W. J., Jr., and L. Moskowitz, A proposed spectral form for fully developed wind seas based on the similarity theory of S. A. Kitaigorodskii, *J. Geophys. Res.*, *69*, 5181–5190, 1964.

Stilwell, D., Jr., Directional energy spectra of the sea from photographs, *J. Geophys. Res.*, *74*, 1974–1986, 1969.

Stilwell, D., Jr., and R. O. Pilon, Directional spectra of surface waves from photographs, *J. Geophys. Res.*, *79*, 1277–1284, 1974.

Thorsos, E. I., The validity of the Kirchhoff approximation for rough surface scattering using a Gaussian roughness spectrum, *J. Acoust. Soc. Am.*, *83*, 78–92, 1988.

Thorsos, E. I., Acoustic scattering from a "Pierson-Moskowitz" sea surface, *J. Acoust. Soc. Am.*, *88*, 335–349, 1990.

Van Vleck, J. H., and D. Middleton, The spectrum of clipped noise, *Proc. IEEE*, *54*, 1–19, 1966.

Yang, C. C., and S. T. McDaniel, Fourth moments of acoustic waves forward scattered by a rough ocean surface, *Waves Random Media*, *1*, 419–439, 1991.

J. Alvarez Borrego, Departamento de Optica, División de Física Aplicada, CICESE, Km. 107 Carretera Tijuana-Ensenada, Ensenada, Baja California, Mexico.